Structural, optical, and electrical properties of TiO_2 thin films deposited by ALD: Impact of the substrate, the deposited thickness and the deposition temperature

Aline Jolivet, Christophe Labbé, Cédric Frilay, Olivier Debieu, Philippe Marie, Bryan Horcholle, Franck Lemarié, Xavier Portier, Clara Grygiel, Sylvain Duprey, et al.

Structural, optical, and electrical properties of TiO_2 thin films deposited by ALD: Impact of the substrate, the deposited thickness and the deposition temperature

Aline Jolivet [a,*], Christophe Labbé [a], Cédric Frilay [a], Olivier Debieu [a,b], Philippe Marie [a], Bryan Horcholle [a], Franck Lemarié [a], Xavier Portier [a], Clara Grygiel [a], Sylvain Duprey [a], Wojciech Jadwisienczak [c], David Ingram [d], Mudit Upadhyay [e], Adrian David [e], Arnaud Fouchet [e], Ulrike Lüders [e], Julien Cardin [a,*]

[a] CIMAP Normandie Université, ENSICAEN, UNICAEN, CEA, UMR CNRS 6252, 6 Boulevard Maréchal Juin, 14050 Caen Cedex 4, France
[b] CIRIMAT, Institut Carnot Chimie Balard CIRIMAT, CNRS-INP-UPS, Université Toulouse 3 Paul Sabatier, 118 Route de Narbonne, F-31062 Toulouse Cedex 9, France
[c] School of Electrical Engineering and Computer Science, Ohio University, Athens, OH 45701, USA
[d] Department of Physics and Astronomy, Ohio University, Athens, OH 45701, USA
[e] CRISMAT Normandie Université, ENSICAEN, UNICAEN, UMR CNRS 6508, 6 Boulevard Maréchal Juin, 14050 Caen Cedex 4, France

ARTICLE INFO

Keywords:
TiO_2
ALD
Polarizability
Growth Model

ABSTRACT

TiO_2 films were deposited by ALD on Si and glass substrates. FTIR analysis reveals an incomplete process for deposition temperatures below 160 °C. The transition from the amorphous to the crystallized anatase phase is observed during the variation of the deposition temperature. Films were uniform and homogeneous, with a crystallization threshold temperature depending on the substrate's nature. This delay in crystallization temperature was highlighted by many characterization techniques and found higher by about 50 °C on glass compared to Si substrate. We have also identified the determining role of the deposition temperature and the thickness in the crystallization process and we propose a growth model, independently of the substrate's nature, using different structural analyses. TiO_2 refractive index (n) and extinction coefficient (k) were studied at various deposition temperature. The evolution of the TiO_2 polarizability (α_{opt}) with material density was determined from n values, showing a large variation of polarizability as a function of material density, in agreement and complementary with other studies. The investigation of the dielectric properties at low frequency shows that the losses and relaxation in TiO_2 decrease with deposition temperature, reaching at 300 °C a high and frequency-independent dielectric constant, close to the one reported for polycrystalline anatase.

1. Introduction

Titanium dioxide (TiO_2) thin films are produced by atomic layer deposition (ALD) since the beginning of the 90's [1]. TiO_2 films can have an amorphous or crystalline structure with anatase or rutile phases, both tetragonal. They are of great interest since their structural, optical, and electrical properties offer flexibility driven by the existence of various specific crystalline phases. TiO_2 can also be found in hexagonal brookite phase, however, it is unstable at atmospheric pressure [2,3], and thus it is not considered here.

The stoichiometric compound, TiO_2 is a wide bandgap semiconductor with interesting optical properties for photoconductivity [4], photocatalysis [5–7], or photovoltaic devices [8], with a 3.2 eV indirect bandgap for the anatase phase, and the rutile phase has a direct bandgap of 3.0 eV, whereas the amorphous phase of between 3.3 and 3.5 eV [7,9–13]. In addition, TiO_2 shows high refractive indexes at 1.95 eV (635.8 nm), between 2.10 and 2.45 for amorphous TiO_2 with increasing density [11,14], 2.49 for anatase [14], and around 2.80 for rutile [15,16], making this material suitable for waveguides [17] and Bragg mirrors for optical filters [18,19].

Then, TiO_2 structural stability and electrochemical properties make it a promising candidate for electrochemical devices, such as Li-ion batteries (LIBs) [20,21]. Its high dielectric constant κ, between 80 and 110 in the rutile phase [22–25] or between 40 and 55 in anatase phase [26,27], makes TiO_2 a suitable material for multilayers devices based on high-κ gate dielectric [28]. TiO_2 has also interesting semiconducting

properties in the anatase phase for photovoltaic [29] or photocatalitic [6,30] applications. Then, the combined optical and electrical properties of anatase TiO_2 lead to promising functionalities such as transparent conductive oxides (TCO) (doped with Nb or Ta for instance) [31,32].

The TiO_2 film growth has been developed by many deposition techniques: Pulsed Laser Deposition (PLD) [33,34], magnetron sputtering [35,36], sol–gel [36,37], or CVD [38,39]. It is accepted that Atomic Layer Deposition (ALD) technique is suitable to deposit numerous materials with a very good layer uniformity, conformality and controllable thicknesses over large area for industrial applications [31,40]. Several precursors with various oxidant agents can be used to produce TiO_2. The most common ones are $TiCl_4$ and $Ti(NMe_2)_4$, respectively [31,41–43]. Another one, titanium isopropoxide ($Ti(O^iPr)_4$), commonly shortened as TTIP is also studied [31,44], and it is chosen in this study due to its ease of use, its low price, chemical stability, ease of maintenance, safety of use and low deposition temperature range (between 150 °C and 300 °C), allowing desired technological processes flexibility [31,45,46].

Among these studies, different substrates are used. One of the most studied is the single crystalline Si substrate because of its well established fabrication method and its extensive use in the microelectronics industry (integrated circuits and transistors) [47,48]. However, deposition on a substrate like glass, having high optical transparency in the visible range, can be required for optical applications including photoelectrochemical cells [49] and TiO_2-based transparent conducting oxides (TCO) [50] devices. While Indium-Tin-Oxide (ITO) is the most used TCO in the microelectronic industry, Nb-doped TiO_2 is a suitable substitute because of its comparable electrical conductivity and transparency [31,50,51]. Furthermore, it was reported that nanolaminate materials containing undoped TiO_2 such as Al_2O_3/TiO_2 [23,52,53], or ZnO/TiO_2 [54,55] can be used for photocatalytic applications [53], solar cells devices [52,54,56], and transparent thermoelectric devices [55], respectively.

It is generally accepted that it is critical to control the crystalline phase of TiO_2 films in the as-deposited state as well as after postgrowth annealing. Indeed, depending on the growth conditions and the substrate used, amorphous or crystallized (anatase or rutile) TiO_2 films can be selectively obtained [2,3]. Typically, the TiO_2 anatase phase dominates for films deposited at lower growth temperatures, although the TiO_2 rutile phase becomes stable when the growth temperature exceeds above ~ 600 °C [10]. However most of the studies focus on the structural properties [57–60], and among them only a few describe a growth model [59,60]. Then we propose here to first investigate these structural properties of TiO_2 thin films deposited by ALD on both Si and glass, which has been already studied but with other precursors [8,61], to finally conclude on a schematic representation of the growth mechanism of TiO_2 thin films via two different deposition parameters, and independently of the substrate's nature. Secondly, which is less common [8], the consequences of this growth mechanism on the optical and electrical properties behaviors are investigated. Then, it is proposed to see the evolution of the refractive index, the gap energy, the extinction coefficient, the polarizability and the relative permittivity, which can confirm and support the first part.

In this context, we compare here the TiO_2 thin films deposited on a crystalline (Si) and an amorphous substrate (glass) under the same deposition conditions. The effect of the deposition temperature (T_D) and the film thickness on the TiO_2 properties are investigated, enabling to get a full overview of the properties of amorphous and anatase TiO_2 thin films and to determine the polarizability evolution versus material density of this material on a broad range. A growth model of TiO_2 is suggested according to the evolution of the T_D and deposited thickness.

2. Materials and methods

Depositions were performed with a Picosun® 200 Advanced ALD system. Titanium isopropoxide (TTIP, 98 %, STREM) was used as the titanium precursor and was kept at 75 °C. TTIP was chosen due to its ease of maintenance and safety of use compared to other precursors such as TDMATi or $TiCl_4$ (see respective safety data sheets and [46]). The oxygen precursor was deionized water at room temperature. The TTIP and H_2O pulses were 0.9 s and 4 s,respectively, separated by 5 s of N_2 gas purge. A typical deposition process involved 250, 500, or 1000 cycles at deposition temperatures (T_D) between 100 °C and 300 °C. The substrates used were Neyco 2 in. (1 0 0) oriented p-type Si wafers and 10 mm × 20 mm D263 Schott glass.

The film thickness, refractive index (n), extinction coefficient (k), and the bandgap (Eg) were determined with a Horiba Jobin-Yvon UVISEL 2 spectroscopic ellipsometer. The experimental ellipsometer function Ic and Is, deriving from classical function Δ and ψ, were recorded with an angle of incidence of 70° and in an energy range of 1.5 to 6 eV (206.6 nm to 826.6 nm, UV–vis-NIR spectral range) with 0.01 eV energy step. The spectroscopic ellipsometry (SE) angles were analyzed with the DeltaPsi2 software with a structural model composed of the substrate surmounted by a TiO_2 layer, topped by a rough layer (if necessary) composed of the material layers and air voids and the whole structure is surrounded by air. The single oscillator Tauc-Lorentz dispersion model was used for the TiO_2 layer while Bruggeman's effective medium approximation was used for the rough layer.

The structural properties of the samples were characterized by X-ray Diffraction (XRD) with a Bruker D8 Discover diffractometer operating with a monochromatic Cu Kα1 radiation (λ = 1.5406 Å).

For transmission electron microscopy (TEM) observations, thin foils were prepared by a focused ion beam (FIB) setup (Dual-beam FEI Helios nanolab 660) with an electron imaging resolution of 0.6 nm at 15 kV (FEG gun), and a FIB resolution of 2.54 nm at 30 kV. TEM experiments were performed using a double corrected cold FEG JEOL ARM 200F microscope, operated at 200 kV. Chemical analyses were carried out with an energy dispersive X-ray JEOL CENTURIO spectrometer and a high angle annular dark-field (HAADF) detector. Combined with a scanning electron system, Z contrast imaging (STEM HAADF with a theoretical spatial resolution of 0.78 Å) as well as chemical mapping (STEM EDX), were obtained at a nanometer scale.

The compositions of the samples were also investigated using Rutherford Backscattering Spectroscopy (RBS) at the Edwards Accelerator Laboratory of Ohio University using a 4.5MV tandem accelerator. Samples, oriented at an angle of 7.5° away from the beam direction, were irradiated with a 2.2 MeV ^4He ion beam. The energy resolution obtained on the sample was 20–30 keV, depending on the depth at which the analysis was performed. The elemental concentrations were calculated by fitting the data using the RUMP simulation software. The density was estimated from the elemental concentration in at./cm^2, divided by the thickness, and the Avogadro number to get the concentration in mol/cm^3, and then each elemental concentration was multiplied by its molar mass and added.

The surfaces of the samples were analyzed by atomic force spectroscopy (AFM) in tapping mode using a Nanoscope III device from Digital Instruments. The RMS roughness was calculated from AFM digitized images with a scan area of 4 μm^2, after images were corrected for flatness using the Nanoscope software.

The thin films structural properties were investigated by Raman spectroscopy using a Jobin Yvon – Horiba Labram HR evolution 300 system equipped with a confocal microscope with a magnification of 100x, and a laser source at 532 nm and a 600 grooves/mm grating resulting in a spectral resolution of 1.7 cm^{-1}. Measurements were recorded at five arbitrary selected positions on the film's surface to statistically minimize mismeasurements caused by the manual focal length adjustment. Although the laser source was non-resonant, a special attention was paid to not anneal the samples in situ under the laser beam, employing a low power density of 0.52 $MW.cm^{-2}$.

Transmission MID-FTIR and FAR-FTIR measurements of films deposited on Si were carried out using a Nicolet™ iS50 FTIR spectrometer at normal and 70° incidence, under a continuous N_2 atmosphere.

The dielectric properties of the films on Si were measured using an Agilent 4284A precision LCR meter in the $10^2 - 10^5$ Hz frequency range. The leakage current was measured using a Keithley Model 4200 Semiconductor Characterization System (4200-SCS). Both measurements were carried out by capacitor structures with an area of 250 × 250 μm^2 created by optical lithography with the lift-off method. The top electrode was Ag, deposited by thermal evaporation with a thickness of around 100 nm, whereas the Si substrate served as the bottom electrode.

3. Results and discussion

3.1. Structural properties

The thicknesses on the Si substrate, measured by SE, are shown in Fig. 1 a) for different T_D values and numbers of ALD cycles. For 250 cycles, the films have an average thickness of 8.74 nm with a standard deviation of 0.77 nm. For 500 cycles, the average thickness is equal to 19.20 nm with a standard deviation of 2.79. For 1000 cycles and for T_D below 225 °C, the average thickness is equal to 35.82 nm, with a standard deviation of 2.31 nm, while for T_D over 225 °C (250 °C and 300 °C), higher thicknesses are observed. This is mainly caused by the presence of a rough surface layer, in contrast to all other films, which is determined by fitting the SE measurements.

The film thicknesses are found to be almost similar for both substrates whatever the number of cycles at a T_D of 200 °C, as well as for all other T_D until 1000 cycles. Fig. 1 inset shows the thicknesses for layers grown on both substrates $T_D = 200$ °C and the corresponding growth per cycle (GPC) parameter (given by the ratio of the thickness vs the number of cycles). The GPC on both substrates are close, however, for the lowest cycle numbers (250 and 500), the GPC values are slightly lower for films deposited on Si (0.38 Å/cycle at 250 and 500 cycles) as compared to the glass substrate (0.48 Å/cycle at 250 cycles and 0.42 Å/cycle at 500 cycles). Note that a GPC around 0.3 Å/cycle is common for TiO_2 deposited by thermal ALD with TTIP and H_2O [31,46,62,63]. This means that the growth seems to be slower in the case of Si substrate compared to the glass substrate in the first deposition cycles [64,65]. For a larger number of cycles, the deposition rate becomes independent of the substrate nature, leading to a similar GPC of 0.30 Å/cycle between 1000 cycles and 2000 cycles on Si and glass.

An RBS analysis has been performed for films deposited on Si at different T_D to determine their chemical composition and density. Fig. 2 (a) shows a typical RBS spectrum corresponding to the 1000-cycles film

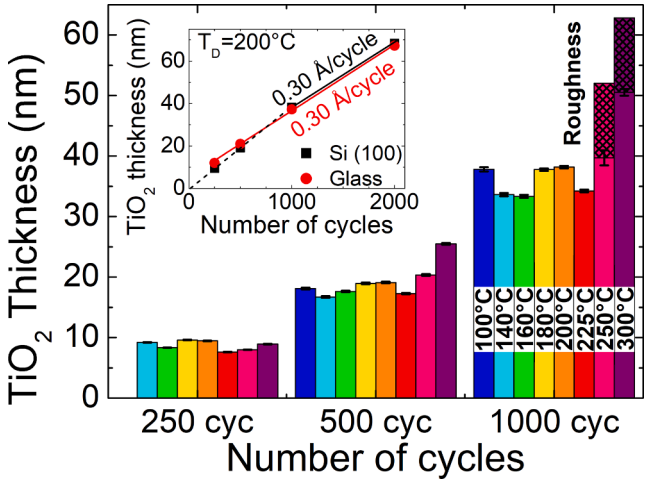

Fig. 1. Thickness of TiO_2 films at various T_D values and for different numbers of cycles on Si(1 0 0) (standard deviation error bar is included on the top of each column). The inset shows the thickness evolution with the numbers of cycles at $T_D = 200$ °C on Si (1 0 0) and glass and the average GPC in Å/cycle. Note that the deposition at 2000 cycles was only done at 200 °C.

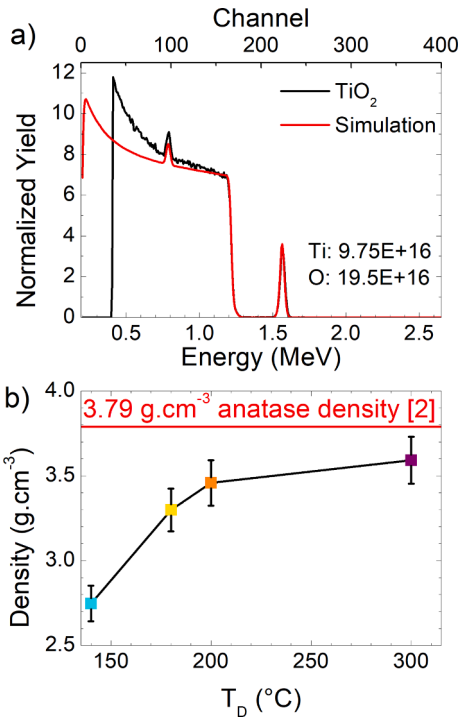

Fig. 2. a) Typical RBS profile of TiO_2 thin film deposited on a silicon wafer with 1000 ALD cycles at 200 °C, and b) corresponding density at different deposition temperatures obtained with RBS data.

deposited at 200 °C along with and the fit curve. It exhibits well-defined peaks of Ti and O above the Si wafer contribution [8,66] and no carbon is detected. The fitting of the experimental data indicates that TiO_2 films deposited at all T_D are stoichiometric. Furthermore, based on the RBS results, the resulting density has been calculated and Fig. 2 (b) shows its behavior as a function of T_D. The density increases with increasing T_D, and reaches 3.59 $g.cm^{-3}$ at a T_D of 300 °C, which remains lower than the bulk TiO_2 anatase phase material density of 3.79 $g.cm^{-3}$ [2] probably due to the crystallization that is not as advanced as for bulk material. This is could reveal a film's densification with increasing T_D, which could be explained by a transition from amorphous to crystallized TiO_2. This point need more characterizations developed below. Please note that due to the composition of the borosilicate glass substrate, which can provide confusing results for the O element content, the RBS measurements for TiO_2 on glass was not conducted.

Fig. 3 shows two sets of STEM EDX and STEM HAADF images of TiO_2 thin films, deposited at 250 °C, on Si (a-d) and glass (e-h) substrates, respectively. The cross sections were observed such that the electron beam was parallel to the film/substrate interface. For both films, the spatial elemental distribution of Ti, O, and Si are represented. Whatever the substrate nature, the distributions are uniform within the whole films suggesting a homogeneous composition of films. There are no elemental composition gradients or segregations at the interface observed, nor a diffusion into the substrates.

A Fourier Transformed IR spectroscopy investigation has been done to get information on films' quality and structure. Fig. 4 (a) presents the Far-FTIR spectra under a normal incidence angle, normalized by the thickness in far-infrared for films on Si substrate. Note that the FTIR analysis of films on the glass substrate is not possible due to the high absorption of the substrate. In Fig. 4 (a), a sharp peak appears at 440 cm^{-1} for T_D above 225 °C, which corresponds to the TiO_2 anatase transverse optical phonon mode TO_3 [67,68]. It depicts also the TO_1 and TO_2 modes of anatase at 260 and 340 cm^{-1}, respectively, appearing only at the T_D value of 225 °C and above. Fig. 4 (b) shows Mid-FTIR spectra for samples tilted with a 70° angle in mid-infrared, enabling activation

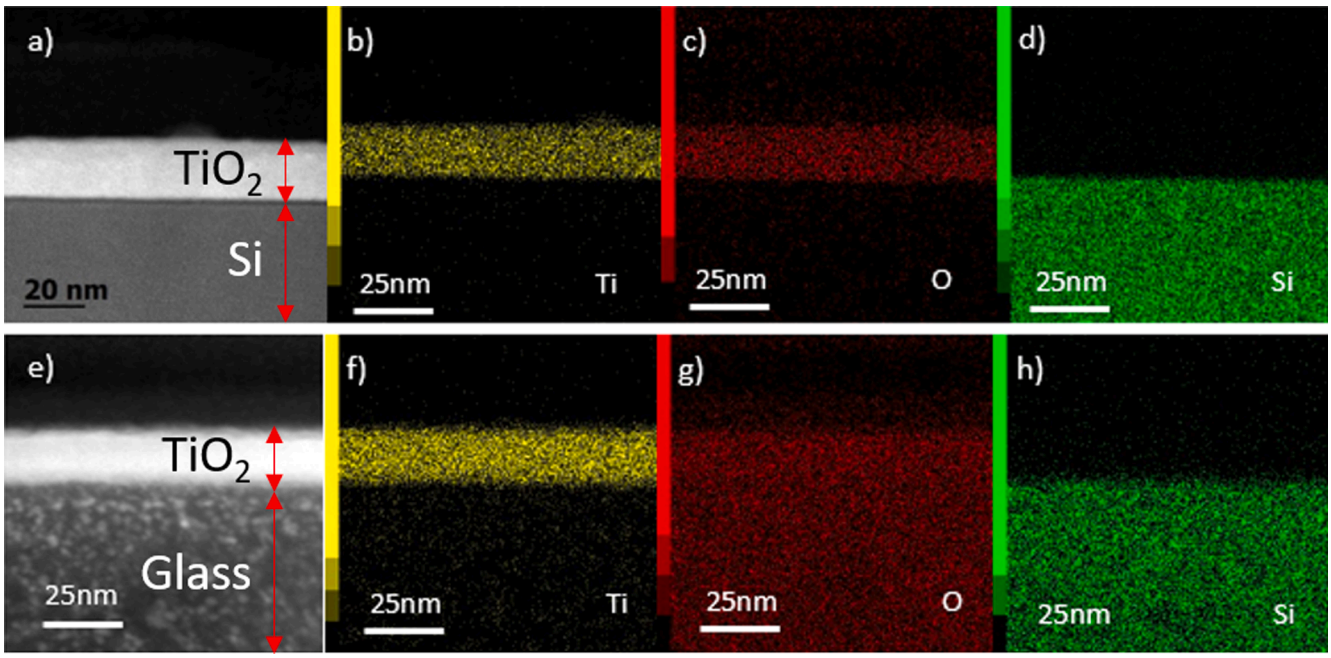

Fig. 3. (a,e) STEM EDX and (b-d) STEM HAADF image of TiO_2 deposited at 250 °C with the corresponding Ti (b,f), O (c,g) and Si (d,h) on Si (1 0 0) and glass substrates, respectively.

of the longitudinal optical modes. Thus, the LO_3 peaks at 855 cm^{-1} are detected, as well as a shoulder around 750 cm^{-1} assigned to the LO_2 modes (both peaks are signatures of the anatase phase). Please note that for this Fig. 4 (b), spectra were normalized with respect to the TO_3 peak at 440 cm^{-1}, to highlight the increase of the LO_3 peak intensities with increasing T_D and the redshift of 5 cm^{-1}, which would indicate a densification coming from a higher crystalline degree in the structure [68,69]. These results support the observed density increase with T_D shown in Fig. 2 (b).

Fig. 4 (c) shows the Mid-FTIR spectra in normal incidence normalized by the film thickness at higher wavenumbers. At lower T_D values (here 100 °C and 140 °C), the presence of hydroxyl group (H—O band) is shown between 3000 and 2900 cm^{-1}, whereas at T_D values above 160 °C, this group disappears [68,70–72]. This hydroxyl group comes either from the water reactant or from the titanium precursor used in the deposition process [44]. Besides, this water content can be at the origin of the lower density observed at lower T_D. Thus, these spectra reveal that a T_D above 160 °C is necessary to obtain a proper ALD cycle without remaining water. For completeness, no organic bands are observed whatever T_D in our work. Such bands were, however already observed in films deposited by ALD with TTIP and water at a lower temperature (90 °C) [73], and are explained by the partial incorporation of the carbon based TTIP ligand residual in the films. These carbon impurities in films can lead to crystallization blocking at lower deposition temperatures as reposted by Xie *et al.* [46]. Since we did not detect any carbon impurities by optical method, XPS analysis was not done in this study, but this is forecast in the future to determine the residual level of the left carbon impurities content in films in our T_D range on both kind of substrate.

Fig. 5 (a) and (b) display the θ-2θ XRD patterns of the 1000 cycles TiO_2 films for Si and glass substrates respectively, as a function of T_D. For both substrates, no peaks are detected up to a T_D of 200 °C, indicating that below this temperature the films are amorphous or contain a very low crystalline content under the detection threshold of the diffractometer. A diffraction peak at 25.2° appears at T_D = 225 °C whose intensity increases progressively with T_D. A second diffraction peak at 48.1°appears only at T_D = 300 °C for both substrates. These two XRD peaks correspond to the TiO_2 anatase phase (space group: $I4_1/amd$, JCPDS: R060277). As a result, crystallization in the anatase phase starts below 225 °C for both substrates and is promoted by increased T_D, in agreement with the literature [60,74,75] with a higher crystalline quality at 300 °C than at 225 °C and 250 °C. Usually, an annealing treatment is required to get the rutile structure [1].

In the light of the XRD results in Fig. 5, and even if the films are homogenous in chemical composition (Fig. 2), films have been investigated further by HRTEM to observe the evolution of TiO_2 structural properties when deposited on both substrates with increasing T_D. Fig. 6 (a) shows an HRTEM image of the TiO_2 thin film grown at 200 °C on the Si substrate. A 2 nm thick amorphous native silicon oxide (SiO_2) is seen at the interface. Above this native silicon layer, an 18 nm thick amorphous film is observed. The enlargement Fig. 6 (b) and the corresponding Fast Fourier Transform (FFT) Fig. 6 (c) confirm this amorphous structure. The Fig. 6 (d) shows an HRTEM image of the TiO_2 film grown at 225 °C on the Si substrate. A 2 nm thick amorphous native silicon oxide (SiO_2) is also seen at the interface. Above this native silicon layer, there is an 18 nm thick amorphous film with a crystallite. This crystallite is wider at the top of the film (around 20 nm) than at the interface with the Si substrate (around 5 nm). The enlargement of this crystallite and the corresponding FFT Fig. 6 (e) and (f) confirm the crystallization in anatase phase (JCPDS: R060277). The Fig. 6 (g) displays an HRTEM image of the TiO_2 film grown at 250 °C on the Si substrate. A 2 nm thick amorphous native silicon oxide is once again seen at the interface. Above this native silicon layer, the film is entirely crystallized, and a single crystalline grain of about 50 nm wide in lateral dimension is seen and its height corresponds to the whole film thickness (~18 nm). No particular orientation relationship between the deposited layer and the Si substrate has been noticed, that could be explained by the presence of the amorphous native oxide layer at the interface, and some of these grains reach up to 100 nm in length (Fig. 6 (j)). Fig. 6 (h) is an enlargement of the squared region in Fig. 6 (g). It shows two sets of perpendicular lattice planes and the FFT shown in Fig. 6 (i) is in good agreement with a [0 0 1] projection of the anatase structure of titanium dioxide (JCPDS: R060277). This confirms the crystallization in anatase up to 225 °C observed in Fig. 5 and is consistent with previous results found in literature [8,31].

On the glass substrate and at the same T_D value of 250 °C (Fig. 6 (a, d,

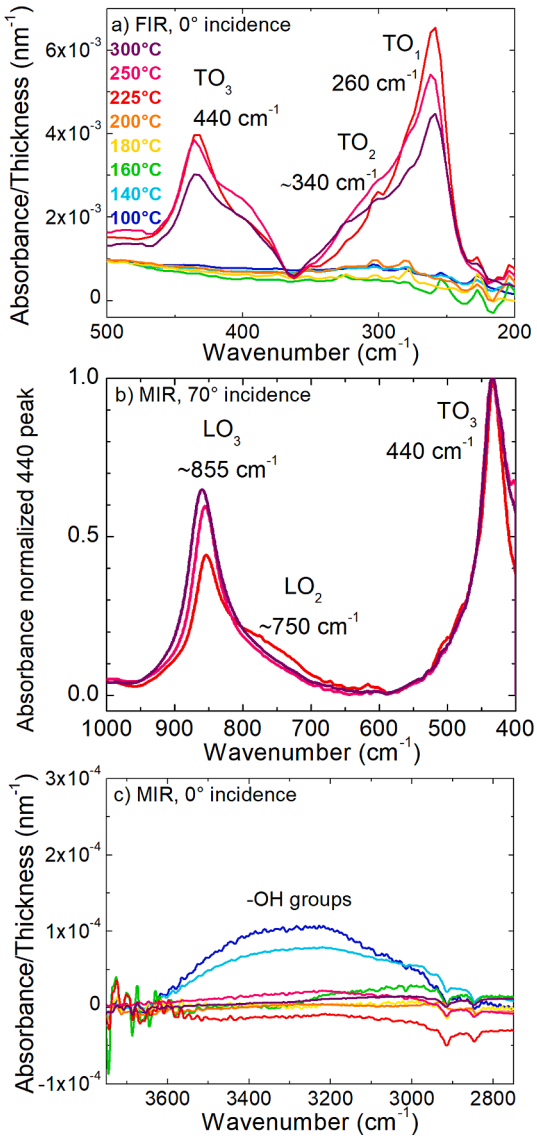

Fig. 4. FTIR Absorbance spectra of 1000 cycles of TiO_2 thin films deposited on silicon between 100 °C and 300 °C, a) FIR with a normal incidence between 500 cm^{-1} and 200 cm^{-1}, b) MIR tilted at 70° between 1000 cm^{-1} and 400 cm^{-1} and c) MIR with a normal incidence between 4000 cm^{-1} and 2700 cm^{-1}.

g, j)), a similar TEM cross-sectional observation has been carried out. The TiO_2 film thickness is also homogeneous with a mean value of about 18 nm similarly to the silicon substrate (Fig. 6 (a, d, g, j)). In a similar way as on the Si substrate at 225 °C, the thin film is here composed of small crystallized grains (here around 30 nm) also in the anatase phase (JCPDS: R060277) embedded in an amorphous matrix, at the top of the film. Fig. 6 (l) and (m) display an enlarged crystalline region of the film and its corresponding FFT pattern, respectively. This latter reveals the presence of (0 1 1) lattice fringes of the TiO_2 anatase structure.

However, at T_D of 300 °C on glass (Fig. 6 (n)), the TEM images reveal that the film is entirely crystallized in the anatase phase (JCPDS: R060277), which is common by ALD for this precursor in this temperature range [31]. The film thickness is still around 18 nm. Fig. 6 (o) and (p) display an enlarged crystalline region of the film and its corresponding FFT pattern, respectively. This latter corresponds to a [1–1–1] projection of the anatase structure.

Thus, despite the presence of the amorphous native oxide on the top of the crystalline Si substrate, and a slightly lower GPC value for low numbers of growth cycles, the Si wafer seems to favor crystallization by

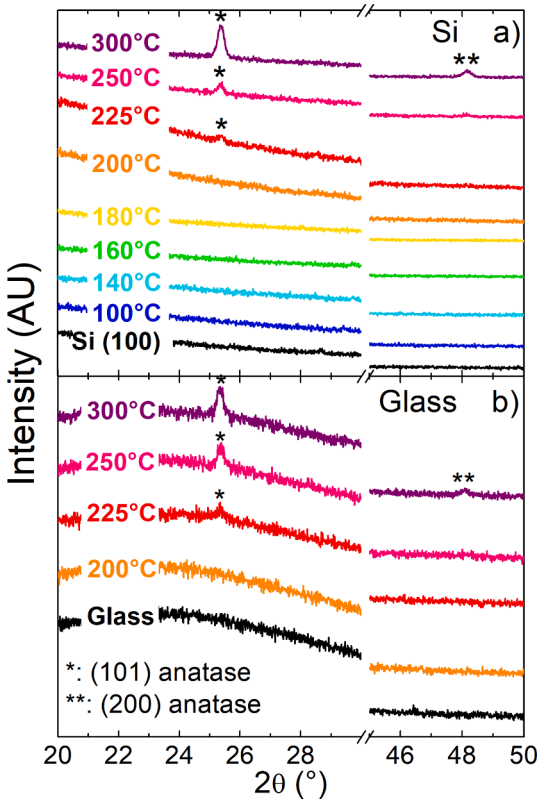

Fig. 5. XRD patterns of 1000 cycles TiO_2 thin films deposited a) on Si (1 0 0) and b) on glass at 100 °C up to 250 °C.

comparison with an amorphous substrate such as glass. This observation is confirmed by Aarik *et al.* [43] and Mitchell *et al.* [76] who reported that crystallization happens immediately on Si substrate without a native oxide layer and, even with a native oxide layer, crystallization starts at a critical thickness of the deposited film. The value of this critical thickness depends on the thickness of the native oxide layer: the thinner the native oxide, the smaller the critical layer thickness [31]. So the observed delay in crystallization of our TiO_2 films deposited on glass compared to the ones deposited on Si is in full agreement with the latter literature reports: films are completely crystallized on Si at a T_D value of 250 °C whereas crystallization is incomplete on glass and fully achieved only at a T_D value of 300 °C.

A Raman spectroscopy study has been done on films deposited on Si and glass substrates with a different number of cycles and T_D values. Fig. 7 (a) displays the evolution of the Raman spectra of 500 and 1000-cycles films deposited on Si. Films deposited at T_D = 200 °C show no Raman peak coming from TiO_2. According to the irreducible representation of the optical lattice vibrations of anatase TiO_2, films deposited above 225 °C for 1000 cycles and 250 °C for 500 cycles, present peaks of anatase: $E_{g(1)}$, $E_{g(2)}$, and $E_{g(3)}$, and $B_{1g(1)}$ [77,78].

On glass, for 1000 cycles films (Fig. 7 (b)), no substrate-related peaks are present. At a T_D value of 200 °C, no film-related peaks are observed, while films deposited at higher T_D (225 °C, 250 °C, and 300 °C) present all the previously cited peaks of anatase: $E_{g(1)}$, $E_{g(2)}$ $E_{g(3)}$, $B_{1g(1)}$ [77,78], plus the $B_{1g(2)}$ and A_{1g} that were hidden by the Si substrate contribution in Fig. 7 (a).

Fig. 8 presents the evolution of the $E_{g(1)}$ peak divided by the film's thickness on Si (left hand panels) and glass (right hand panels) for 500 and 1000 cycles. The 1000-cycles films show anatase Raman vibration modes when deposited above 225 °C on both substrates and which gain in intensity with T_D on Si. For 500 cycles, peaks appear only above 250 °C on Si and at 300 °C on glass. Therefore, the film crystallization starts below 225 °C as observed in FTIR spectra (Fig. 4) and in XRD

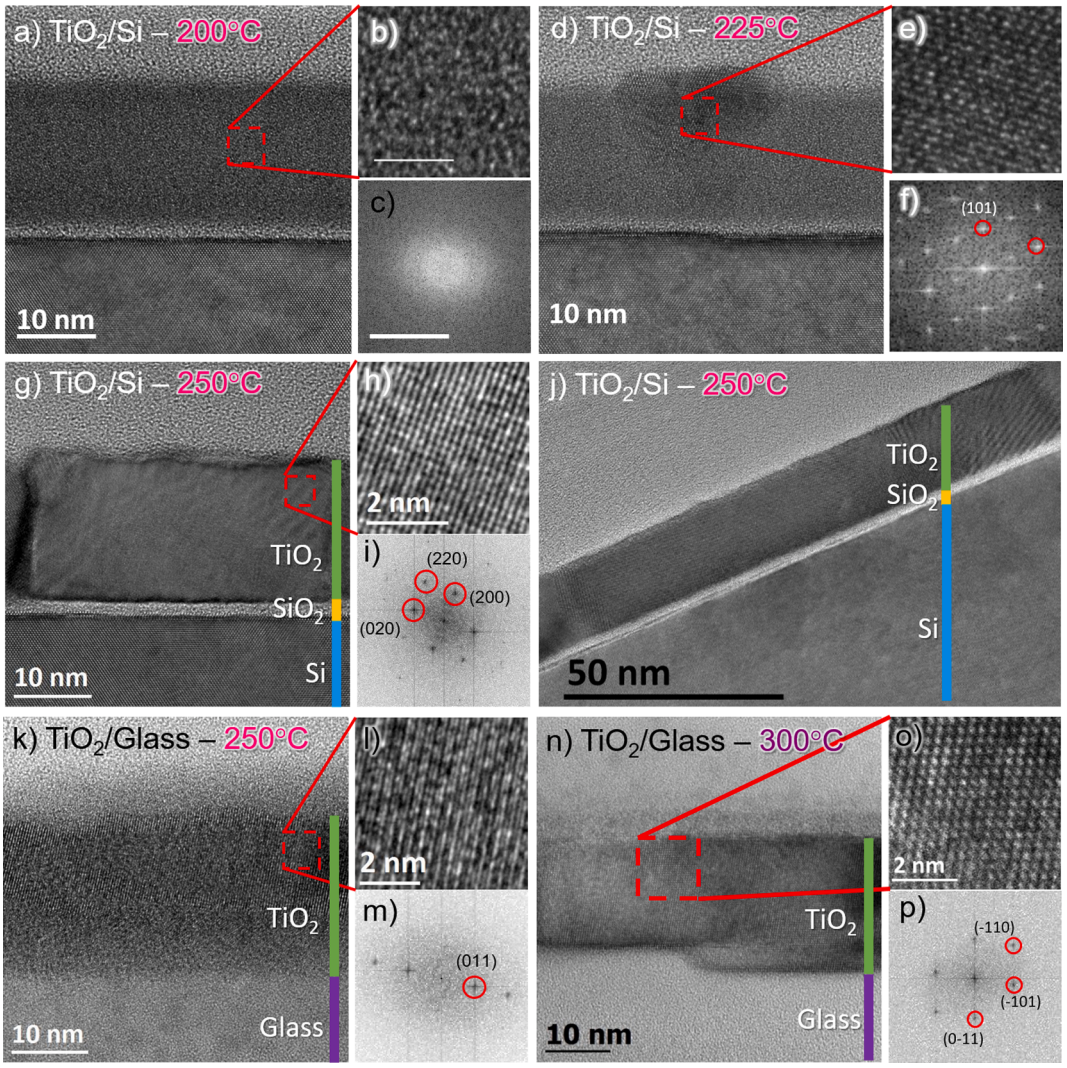

Fig. 6. (a) High-resolution TEM image of a TiO_2 thin film grown by ALD at 200 °C on a Si (1 0 0) substrate with native amorphous silica at the interface between Si and TiO_2; (b) enlarged region showing an amorphous structure and (i) Fast Fourier Transform (FFT) consistent with an amorphous of TiO_2. (d) HRTEM image of a TiO_2 thin film grown by ALD at 225 °C on a Si (1 0 0) substrate with native amorphous silica at the interface between Si and TiO_2 and a crystallite surrounded by amorphous TiO_2; (e) enlarged region showing lattice planes of the crystallite and (i) Fast Fourier Transform (FFT) consistent with a [-1–11] projection of the anatase structure of TiO_2. (g) High-resolution TEM image of a TiO_2 thin film grown by ALD at 250 °C on a Si (1 0 0) substrate with native amorphous silica at the interface between Si and TiO_2; (h) enlarged region showing two sets of perpendicular lattice planes and (i) Fast Fourier Transform (FFT) consistent with a [0 0 1] projection of the anatase structure of TiO_2. (j) same sample as (g) but enlarged picture with a 100 nm length crystallite. (k) HRTEM image of a TiO_2 thin film grown by ALD at 250 °C on a glass substrate; (l) enlarged region showing two sets of perpendicular lattice planes and (m) corresponding FFT with the presence of (0 1 1) lattice fringes of the TiO_2 anatase structure. (n) HRTEM image of a TiO_2 thin film grown by ALD at 300 °C on a glass substrate, (the step at the interface is due to the glass' surface); (o) enlarged region showing two sets of perpendicular lattice planes and (p) corresponding FFT with a [1–1–1] projection of the anatase structure of TiO_2.

diagrams (Fig. 5) and is promoted by the film's thickness. Furthermore, for the 1000-cycles films, the $E_{g(1)}$ peak is less intense on glass than on silicon for the same temperatures, meaning that crystallization is sensitive to the substrate nature and there is a need for a higher thermal budget on glass, an amorphous substrate, than on silicon, a single crystalline substrate. This was already observed by the TEM analysis in Fig. 6. Therefore, crystallization is promoted not only by the T_D via the nature of the substrate but also by the increase in thickness, as already observed in the literature [43,60,75]. Thus, these results highlight a delay effect in crystallization on glass compared to the one on Si: the T_D value has to reach 300 °C for 500 cycles and 250 °C for 1000 cycles to have the $E_{g(1)}$ peak on glass, whereas it is 250 °C and 225 °C on Si, respectively. Then, this $E_{g(1)}$ peak is at 141 cm^{-1} instead of 144 cm^{-1} in the literature for bulk anatase [77,78], this shift in position can be linked to the crystallization that is not as advanced as for bulk material as seen in the density estimated from RBS analysis Fig. 2 (b).

To complete the structural investigation, the films have been analyzed by AFM at different T_D values and for various ALD numbers of cycles. The AFM images for the films deposited at 250, 500, and 1000 cycles on silicon and on glass are presented in Fig. 9 a) and b), respectively. The Root Mean Square (RMS) roughness estimated from the AFM images is displayed in Fig. 10. Specifically, for films on Si deposited with 250 cycles, all films present smooth surfaces with an RMS roughness of 0.5 nm independent of the T_D (Fig. 9 (a)). For the two larger cycle numbers, at 180 °C, the RMS roughness does not changed significantly, confirming the smooth surface, but from 200 °C to 225 °C especially for the 1000 cycles number, the roughness increases considerably up to 2–2.5 nm, with grains appearing at the film's surface. Finally, at 250 °C and 300 °C, the roughness increases respectively up to 4 and 5.5 nm. This behavior is consistent with the SE analysis shown in Fig. 1. Concerning the glass substrate (Fig. 9 (b)), the behavior is similar to on Si, but the roughness remains on the whole lower and exceeds 1 nm only up

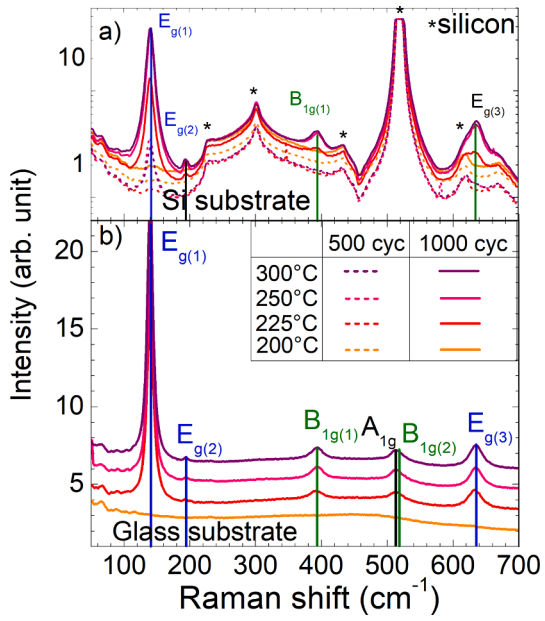

Fig. 7. Raman spectra of TiO_2 deposited on a) Si substrate with 500 and 1000 cycles and b) glass substrate with 1000 cycles between 200 °C and 300 °C.

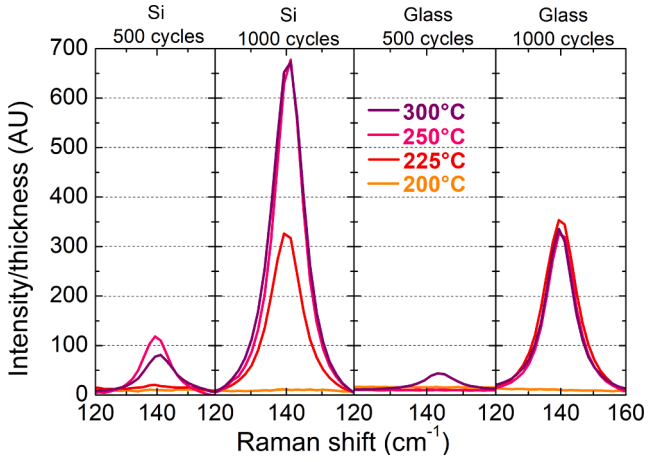

Fig. 8. Raman spectra intensity of the $Eg_{(1)}$ peak for Si and glass substrates at different T_D values divided by the films' thickness.

to 225 °C.

Consequently, the RMS roughness increases independently of the substrate with increasing the T_D and the number of cycles, *i.e.* the thickness. At the same time, we observed that the film roughness increases slower on glass than on Si substrate when the T_D or the thickness change. Therefore, a delay in the observation of the roughness depends on the T_D and the thickness. Such surface behaviors can be linked to the TiO_2 phase changing between the amorphous and anatase phases, already observed by XRD, TEM, and Raman analysis. Indeed, we have observed that this crystallization occurs irrespective of the substrate and is accentuated by increased film thickness, but with a delay effect in complete film crystallization for a glass substrate with the T_D increase. Thus, the TiO_2 film surface properties seem to reflect the crystalline ordering of the thin films, with a slightly enhanced crystallization temperature for the films on glass.

However, at 1000 cycles on Si substrate the film's grain size is increasing with T_D between 200 °C and 250 °C (Fig. 9 (a), reaching grains of 0.3 μm at 250 °C), and then decreasing at 300 °C (0.1 μm). This decreasing in grain size between 250 °C and 300 °C has already been observed by Lee *et al.* [59] and is explained by a lower surface nucleated density at low T_D (≤250 °C) than at higher T_D (≥300 °C). Indeed, at low T_D (≤250 °C) the nucleation sites are far from each other, and grains can expand freely laterally, whereas at high T_D (≥300 °C) there are more nucleation sites, so growing grains are surrounded by other growing grains and the crystal growth mechanism is dominated by Ostwald ripening.

Then, the crystallization depends on three factors:

i) *The deposition temperature:* T_D value has a strong influence on the crystallization, with an anatase crystallized film at 250 °C on Si, and at 300 °C on glass. The TiO_2 crystallization in the anatase phase at a T_D value as low as 250 °C has already been observed in earlier studies [60,74,75]. However, the structural analysis shows that crystallization on Si is of higher quality at T_D = 300 °C than at 250 °C (FTIR Fig. 4 and XRD Fig. 5). Furthermore, the higher the T_D, the more nucleation sites there are, leading to smaller crystallites at high temperature than at lower temperature (but still high enough to allow crystallization) as each crystallite hinders the growth of the others [59].

ii) *The deposited film's thickness*: the increase of thickness promotes crystallization [59,60], with the existence of a critical thickness above which crystallization can occur. This is due to the fact that the interface or surface energy of amorphous TiO_2 is lower than the one of crystallized TiO_2 and vice versa for the bulk Gibbs free energy. When the critical thickness is reached, the difference between crystallized and amorphous bulk Gibbs free energy can compensate the difference between surface energies and thus allowing crystallization, as explained more in details by Nie *et al.* [79] for a similar growth with HfO_2.

iii) *The nature of the substrate*: a shift in T_D regarding the crystallization on glass substrate has been observed compared to the Si substrate for the same thickness (constant number of cycles). As the film deposition using ALD is considered as steady-state, it means that it is the surface energy of Si and glass substrates that is responsible for this observed shift [31].

These results are in accordance with the literature for TiO_2 deposited by ALD [31,60] and are now confirmed for TiO_2 deposited on different substrates (crystallized vs amorphous), showing the necessity of a higher T_D for TiO_2 on amorphous substrates to obtain the same material's crystalline quality [31,43,76].

The characterizations of this study explicitly demonstrates that the crystallization is triggered by a specific growth mechanism already proposed for anatase TiO_2 in the literature [43,60,75,76]. The pictorial summary of these growth mechanisms is shown in Fig. 11 whatever the substrate. In the early growth stages all deposited TiO_2 films are amorphous. Then, when a certain thickness is reached, some nucleation sites are formed at the film's surface, as seen in AFM images (see Fig. 9). These nucleation sites grow with the newly deposited matter, also with the surrounding amorphous host evolution (see TEM image Fig. 6 (d) and (k)). In the final step, the TiO_2 film becomes entirely crystallized as seen in Fig. 6 (g) for Si substrate or Fig. 6 (n) for glass substrate. In the same way, the nucleation process is also promoted by the T_D increase.

3.2. Optical properties

An optical properties characterization of the films has also been carried out, starting with SE measurements for the determination of the refractive index *n* and the extinction coefficient *k*. Fig. 12 shows the evolution of *n* and *k* between 1.5 and 6 eV for two samples deposited with 500 cycles on Si, at a T_D value of 200 °C (amorphous films), and at 250 °C and 300 °C (crystallized film in anatase phase). *n* and *k* of the two crystallized samples merge with the estimated uncertainties but they are well distinguishable from the amorphous ones considering the associated uncertainties range. At energies below the TiO_2 anatase band gap of 3.2 eV [7], the crystallized TiO_2 presents a higher *n* than that of the amorphous one. This observation is different for energies higher than 4.5 eV, where *n* of the anatase film falls below the one of the amorphous film. On the other hand, *k* of anatase is always higher than the one of

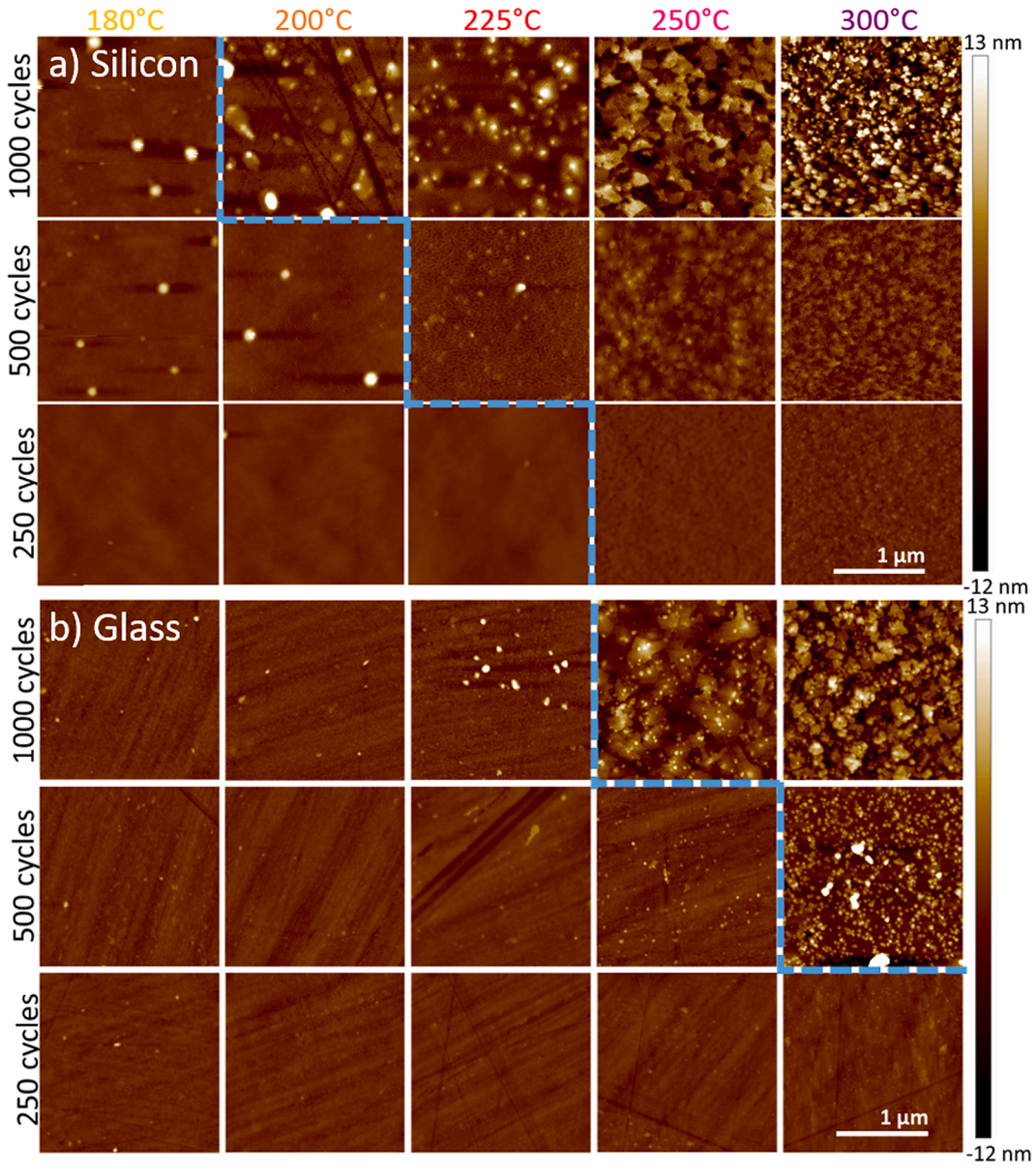

Fig. 9. AFM images of TiO_2 deposited a) on Si and b) glass substrate from 180 °C to 300 °C. AFM images are 2 µm × 2 µm.

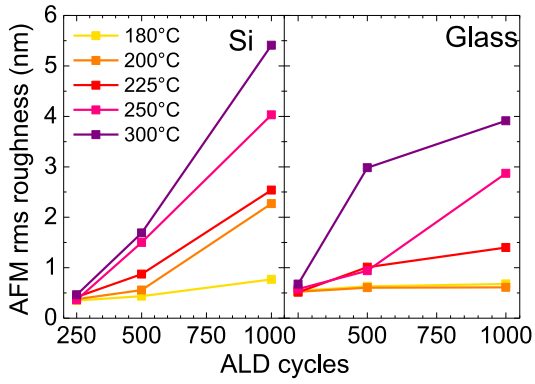

Fig. 10. AFM RMS roughness of TiO_2 deposited on a silicon substrate from 180 °C to 300 °C for various number of ALD cycles.

amorphous TiO_2 in the energy range studied here (1.5 to 6 eV). This observation has to be nuanced by the fact that for energies higher than 5 eV, the curves and their uncertainties are not well distinguishable from each other.

A closer look at n and k for films deposited on Si and glass is given in Fig. 13, which shows the behavior of n (Fig. 13 (a)) and k (Fig. 13 (b)) as a function of the T_D value at 1.95 eV (low absorption range) and 4 eV (high absorption range).

The n @ 1.95 eV are consistent, taking into account the uncertainties, with the literature of thin films, that gives about 2.25 for amorphous films deposited at 100 °C and 2.49 for anatase films deposited at 300 °C [80,81]. n seems to reach a plateau after a T_D value of 250 °C on Si at both energies. This increase of n with T_D and the plateau after crystallization was observed by J. Aarik *et al.* [80], L. Aarik *et al.* [81], and M. H. Suhail *et al.* [82]. This effect is explained by the increasing density of TiO_2 films with increasing T_D agrees well with RBS (Fig. 2) [74,80,83,84]. For the glass substrate, n is also increasing with T_D, even after 250 °C, until it reaches the value of 2.40 at 300 °C, close to the one on Si substrate. At all lower T_D values, n for Si is always higher than the one for glass at both energies. This systematic difference in the n values

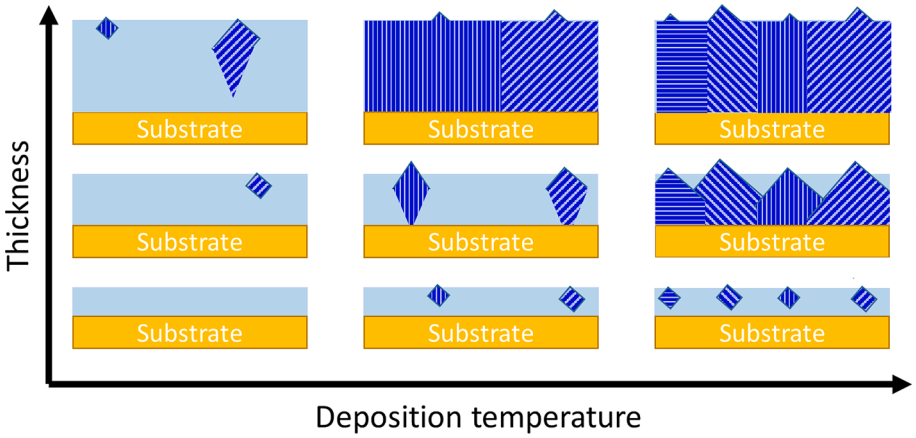

Fig. 11. Schematic representation of TiO_2 film growth mechanism driven by the deposition temperature T_D and the thickness.

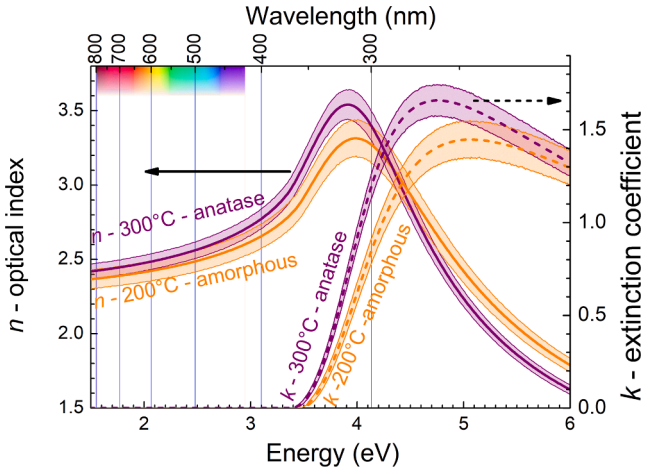

Fig. 12. Refractive index n and extinction coefficient k measured by ellipsometry for a Si substrate with 500 cycles number, for an amorphous and anatase TiO_2 phase, respectively at T_D values of 200 °C and 300 °C, in an energy range of 1.5 to 6 eV (206.6 nm to 826.6 nm, UV–vis-NIR spectral range). The n and k uncertainties are symbolized by the bands.

between the two substrates can be linked to the delay in crystallization observed and discussed above. At 300 °C, films are fully crystallized in anatase for both substrates and both *n* converge logically towards the same value.

The *k* value (Figs. 12 and 13) is low (near zero) before the band gap at 1.95 eV, and increases with T_D at 4 eV, independently of the phase and the substrate nature. This increase is characteristic of the crystallization in anatase phase [82]. The *k* values increase remains less pronounced for glass than for Si, probably highlighting the delay of crystallization between Si and glass substrates. Note that, at 300 °C, *k* values for Si and glass remain different whereas *n* trends are similar, even if one considers that the values of *k* and their associated uncertainties for both substrates are coming together.

The band-gap energies E_g obtained by SE on Si and glass substrates are represented in Fig. 14 using the Tauc-Lorentz dispersion formula. A quasi-identical band gap energy behavior with T_D is visible for both substrates. E_g values for Si substrate are decreasing with T_D from 3.5 eV (value close to the ones of amorphous TiO_x ranging from 3.3 to 3.5 eV [11–13]) down to 3.2 eV at 300 °C (value commonly assigned to the indirect band-gap of TiO_2 anatase in the literature [7]). For glass substrate, E_g values are decreasing from 3.7 down to 3.4 at 300 °C, reaching the same value as for Si at 250 °C, thus illustrating the delay of crystallization for glass. This difference in gaps at 300 °C between Si and

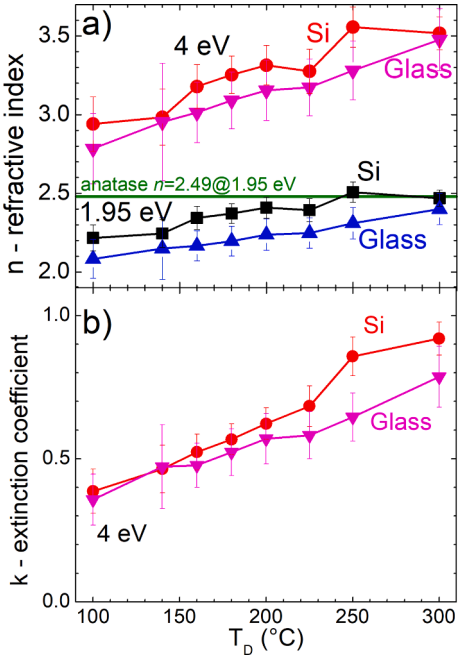

Fig. 13. a) Refractive index n and b) extinction coefficient k at 1.95 eV (636 nm) and 4 eV (310 nm) for Si and glass substrates from 100 °C to 300 °C.

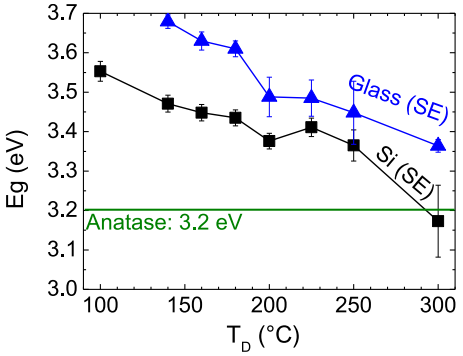

Fig. 14. Energy bandgap vs T_D temperatures for TiO_2 films deposited for 1000 cycles on Si and glass substrates determined from spectroscopic ellipsometry (SE) measurements.

glass substrates is due to the fact that k are also different at this T_D value whereas n is the same. So, even if the structural analyses (XRD in Fig. 5 (b), TEM in Fig. 6 (n)), are indicating an anatase TiO_2, the crystallization process is less advanced in the case of glass at the same T_D value, as seen by Raman spectroscopy (Fig. 8). The similar evolution of E_g for different substrates (silicon and glass) implies that TiO_2 thin films deposited by ALD on both substrates converges towards similar electronic, and therefore optical properties with T_D [13]. The decrease of E_g with increasing T_D was reported before and is usually explained by the progressive organization of the amorphous structure obtained at the lowest temperatures towards a crystallized one with increasing T_D, and this is consistent with the fact that amorphous TiO_2 has a wider energy band gap than anatase TiO_2 [80].

The polarizability describes the response to how matter, subjected to an electric field, acquires an electric dipole moment proportional to that applied field. Such response is directly at the origin for a material's dielectric constant (*i.e.* refractive index) and is therefore specific for each material. The molecular optical polarizability α_{opt} of the samples can be determined from the Lorentz-Lorenz equation [85,86]:

$$\alpha_{opt} = \frac{3}{4\pi}\frac{M_{TiO_2}}{\rho N_A}\frac{n^2-1}{n^2+2} \quad (1)$$

where M_{TiO2} is the molar mass of TiO_2 (79.865 g/mol), ρ is the density determined by RBS (Fig. 2 (b)), and n@2.26 eV (550 nm) of the films deposited at different T_D at values. α_{opt} is depicted in red as a function of T_D in Fig. 15 (a) and as a function of the density in Fig. 15 (b). For comparison, α_{opt} from Piercy *et al.* [85] who also studied mixed amorphous/anatase and anatase films produced by ALD but using $TiCl_4$ precursor and water are also plotted. Fig. 15 (a) shows, in the present work, that α_{opt} decreases from $6.8.10^{-24}$ cm^{-3} to $5.6.10^{-24}$ cm^{-3} with T_D increasing from 140 °C to 200 °C. Then, one can see that the crystallization effect occurring between 200 °C and 300 °C is correlated with the polarization becoming rather constant at $5.6.10^{-24}$ cm^{-3}. Concerning the polarizability behavior with density (Fig. 15 (b)), it monotonously decreases with material's density increase. The estimated polarizability values are similar to the one reported by Piercy *et al.*, except that they were shifted in T_D (Fig. 15 (a)). This can be explained by the difference between the precursors ($TiCl_4$ instead of TTIP) and a different ALD apparatus. Whatever the experimental reasons, the two evolutions of α_{opt} with the density, a parameter that is not set-up dependent, (Fig. 15 (b)) are consistent and complement each other. Therefore, the polarizabilities calculated in this work are matching well the literature [85,86] and depict that optical polarizability can be tuned with the material's density.

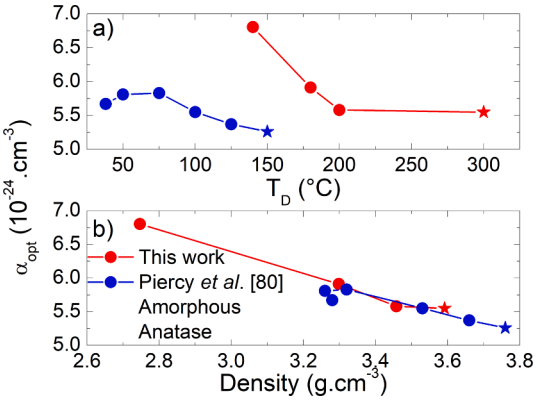

Fig. 15. Optical molecular polarizabilities at 550 nm of TiO_2 deposited between 140 °C and 300 °C on Si substrate (this work in red), and by ALD with $TiCl_4$ and water between 100 °C and 150 °C (Piercy et al. [85] in blue). (For interpretation of the references to colour in this figure legend, the reader is referred to the web version of this article.)

3.3. Electrical properties

The relative permittivity (ε_r) and the dielectric losses (tan δ) of TiO_2 deposited on Si with 1000 cycles at various T_D values are shown in Fig. 16(a) and 16(b). Note that the electrical analysis does not allow measurements for the film deposited on glass because the substrate is used as an electrode and so has to be conductive. The relative permittivity ε_r is T_D dependent, thus increasing with it (Fig. 16(a)). It is seen that for the amorphous film deposited T_D equals to 200 °C, the ε_r is decreasing with increasing frequency from 10.6 @10^2 Hz to 1.8 @10^5 Hz. For the film deposited at a T_D of 250 °C, already being crystallized in anatase phase, the same behavior is observed between 32 @10^2 Hz to 11 @10^5 Hz, however the ε_r value is noticeable higher. Only the TiO_2 film in anatase phase deposited at T_D of 300 °C a relative permittivity ε_r is almost independent from the frequency between 62 @10^2 Hz to 55 @ 10^5 Hz, and its values is close to the one of bulk anatase [27]. These values of ε_r are close to the ones found elsewhere *i.e.* about 10 and 33 for amorphous TiO_2 and between 70 and 80 for anatase [61,86]. The frequency behavior indicates some dielectric relaxation in the films deposited at 200 and 250 °C, while the film at 300 °C shows the typical independent frequency behavior expected for a high-quality TiO_2 film [87].

The loss tan δ value (Fig. 16(b)) is decreasing with increasing T_D, confirming the existence of relaxation for the films deposited at lower T_D. However, it remains stable for all T_D under 0.5, indicating a low density of defects in TiO_2 and is consistent with values for other TiO_2 in the litterature [87–90]. At 200 °C, tan δ increases from 0.26 @10^2 Hz and 0.45 @8.10^3 Hz and decreases slightly down to 0.37 @10^5 Hz. At 250 °C, tan δ increases from 0.13 @10^2 Hz to 0.31 @10^5 Hz. At 300 °C, tan δ starts by decreasing from 0.21 @10^2 Hz to 0.03 @6.10^3 Hz and then increases until 0.09 @10^5 Hz.

The dielectric properties presented in Fig. 16 show that the T_D increase induces lower losses and a relaxation in TiO_2, reaching a high and frequency-independent dielectric constant at 300 °C close to the one of polycrystalline anatase [27]. This can be related to the high crystalline quality observed by other techniques, like the good chemical stoichiometry of the films also observed by RBS analysis (Fig. 2). The lower losses and so the lower defect density at T_D = 300 °C on Si substrate means that the film is of higher crystalline quality at this T_D, thus confirming the structural analysis by FTIR spectroscopy and XRD (Fig. 4 and Fig. 5 respectively).

4. Conclusion

The growth of TiO_2 thin films grown on silicon (1 0 0) substrate and D263 glass by ALD from TTIP and water was studied. According to TEM, XRD, AFM, FTIR, and Raman analyses, the films start their

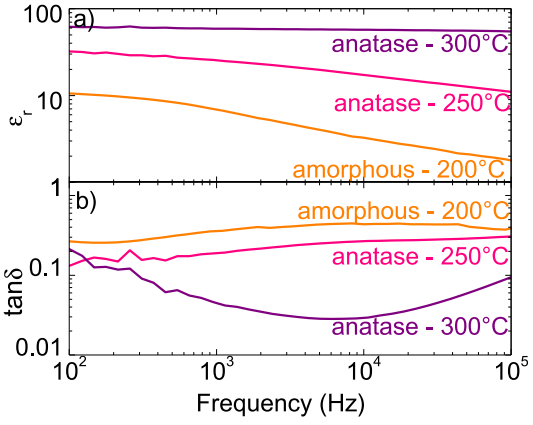

Fig. 16. a) Relative permittivity and b) loss of 1000 ALD cycles of TiO_2 at 200 °C, 250 °C, and 300 °C deposited on Si.

crystallization process between 200 °C and 225 °C in the anatase phase. Randomly orientated grains grow with increasing T_D resulting in an increase of the film density and roughness. Film growth follows then known successive stages that are fully evidenced in this work: amorphous films are formed in the early growth stage, then crystallized nuclei appear at the top surface, and finally the growth of these nuclei towards the deposited matter, until the entire crystallization of the film occurred. This crystallization process is enhanced by increasing T_D and the film's thickness (*i.e.* number of cycles), whatever the substrate nature. However, the Si crystallized substrate promotes crystallization compared to an amorphous one such as glass. We have highlighted a delay effect in crystallization with the T_D increase of almost 50 °C on glass compared to the one on Si and investigated by many different characterizations. The optical characterizations are showing a band gap of 3.2 eV when the films are fully crystallized, consistent with the one reported for bulk anatase. Furthermore, the optical molecular polarizability of the films was calculated from RBS densities and refractive indices, using the Lorentz-Lorenz relation. The obtained polarizabilities are consistent with the values found in the literature and gave a further inside into the polarizability versus density evolution. At last, TiO_2 deposited at 300 °C has good dielectric properties in terms of dielectric constant (~60) and losses (~0.03) without relaxation.

Aline Jolivet: Writing – original draft, Writing – review & editing, Investigation, Data curation. **Christophe Labbé:** Visualization, Supervision, Investigation, Writing – original draft. **Cédric Frilay:** Resources, Data curation. **Olivier Debieu:** Investigation, Data curation. **Philippe Marie:** Data curation. **Bryan Horcholle:** Software. **Franck Lemarié:** Data curation. **Xavier Portier:** Data curation. **Clara Grygiel:** Data curation. **Sylvain Duprey:** Data curation. **Wojciech Jadwisienczak:** Data curation. **David Ingram:** Data curation. **Mudit Upadhyay:** Data curation. **Adrian David:** Validation. **Arnaud Fouchet:** Validation. **Ulrike Lüders:** Validation. **Julien Cardin:** Formal analysis, Investigation, Writing – original draft, Visualization, Supervision.

The authors declare the following financial interests/personal relationships which may be considered as potential competing interests: The authors would like to acknowledge financial support from the CNRS prematuration project CoCOT, and the Normandie region through the projects RIN PLDsurf. X. Portier acknowledges CNRS Federation IRMA - FR 3095 and the ANR EQUIPEX "GENESIS" grant "ANR-11-EQPX-0020" in the frame of the "Investissements d'avenir" whose funding allowed the acquisition of the FIB setup (FEI Helios nanolab 660 equipment).

Data will be made available on request.

The authors are thankfull to O. Marsan (Cirimat) for Raman band positions verifications, and to Air liquid for the support. The authors would like to acknowledge financial support from the CNRS prematuration project CoCOT, and the Normandie region through the projects RIN PLDsurf.

X. Portier acknowledges CNRS Federation IRMA - FR 3095 and the ANR EQUIPEX "GENESIS" grant "ANR-11-EQPX-0020" in the frame of the "Investissements d'avenir" whose funding allowed the acquisition of the FIB setup (FEI Helios nanolab 660 equipment).

References

[1] M. Ritala, M. Leskela, L. Niinisto, P. Haussalo, Titanium isopropoxide as a precursor in atomic layer epitaxy of titanium dioxide thin films, Chem. Mater. 5 (1993) 1174–1181, https://doi.org/10.1021/cm00032a023.
[2] S.-D. Mo, W.Y. Ching, Electronic and optical properties of three phases of titanium dioxide: Rutile, anatase, and brookite, Phys. Rev. B. 51 (1995) 13023–13032, https://doi.org/10.1103/PhysRevB.51.13023.
[3] A. Di Paola, M. Bellardita, L. Palmisano, Brookite, the Least Known TiO2 Photocatalyst, Catalysts. 3 (2013) 36–73, https://doi.org/10.3390/catal3010036.
[4] M.A. Henderson, A surface science perspective on TiO2 photocatalysis, Surf. Sci. Rep. 66 (2011) 185–297, https://doi.org/10.1016/j.surfrep.2011.01.001.
[5] C.-S. Lee, J. Kim, G.H. Gu, D.-H. Jo, C.G. Park, W. Choi, H. Kim, Photocatalytic activities of TiO2 thin films prepared on Galvanized Iron substrate by plasma-enhanced atomic layer deposition, Thin Solid Films. 518 (2010) 4757–4761, https://doi.org/10.1016/j.tsf.2010.01.015.
[6] V. Pore, A. Rahtu, M. Leskelä, M. Ritala, T. Sajavaara, J. Keinonen, Atomic Layer Deposition of Photocatalytic TiO2 Thin Films from Titanium Tetramethoxide and Water, Chem. Vap. Depos. 10 (2004) 143–148, https://doi.org/10.1002/cvde.200306289.
[7] M. Pelaez, N.T. Nolan, S.C. Pillai, M.K. Seery, P. Falaras, A.G. Kontos, P.S. M. Dunlop, J.W.J. Hamilton, J.A. Byrne, K. O'Shea, M.H. Entezari, D.D. Dionysiou, A review on the visible light active titanium dioxide photocatalysts for environmental applications, Appl. Catal. B Environ. 125 (2012) 331–349, https://doi.org/10.1016/j.apcatb.2012.05.036.
[8] W. Chiappim, G.E. Testoni, R.S. Moraes, R.S. Pessoa, J.C. Sagás, F.D. Origo, L. Vieira, H.S. Maciel, Structural, morphological, and optical properties of TiO2 thin films grown by atomic layer deposition on fluorine doped tin oxide conductive glass, Vacuum. 123 (2016) 91–102, https://doi.org/10.1016/j.vacuum.2015.10.019.
[9] T. Siefke, S. Kroker, K. Pfeiffer, O. Puffky, K. Dietrich, D. Franta, I. Ohlídal, A. Szeghalmi, E.-B. Kley, A. Tünnermann, Materials Pushing the Application Limits of Wire Grid Polarizers further into the Deep Ultraviolet Spectral Range, Adv. Opt. Mater. 4 (2016) 1780–1786, https://doi.org/10.1002/adom.201600250.
[10] S.C. Pillai, P. Periyat, R. George, D.E. McCormack, M.K. Seery, H. Hayden, J. Colreavy, D. Corr, S.J. Hinder, Synthesis of High-Temperature Stable Anatase TiO2 Photocatalyst, J. Phys. Chem. C. 111 (2007) 1605–1611, https://doi.org/10.1021/jp065933h.
[11] S. Ratzsch, E.-B. Kley, A. Tünnermann, A. Szeghalmi, Influence of the oxygen plasma parameters on the atomic layer deposition of titanium dioxide, Nanotechnology. 26 (2) (2015) 024003.
[12] S.-J. Park, J.-P. Lee, J.S. Jang, H. Rhu, H. Yu, B.Y. You, C.S. Kim, K.J. Kim, Y.J. Cho, S. Baik, W. Lee, In situcontrol of oxygen vacancies in TiO2by atomic layer deposition for resistive switching devices, Nanotechnology. 24 (29) (2013) 295202.
[13] K. Eufinger, D. Poelman, H. Poelman, R. De Gryse, G.B. Marin, Photocatalytic activity of dc magnetron sputter deposited amorphous TiO2 thin films, Appl. Surf. Sci. 254 (2007) 148–152, https://doi.org/10.1016/j.apsusc.2007.07.009.
[14] J.D.B. Bradley, C.C. Evans, J.T. Choy, O. Reshef, P.B. Deotare, F. Parsy, K. C. Phillips, M. Lončar, E. Mazur, Submicrometer-wide amorphous and polycrystalline anatase TiO_2 waveguides for microphotonic devices, Opt. Express. 20 (2012) 23821, https://doi.org/10.1364/OE.20.023821.
[15] J.R. DeVore, Refractive Indices of Rutile and Sphalerite, JOSA. 41 (1951) 416–419, https://doi.org/10.1364/JOSA.41.000416.
[16] B. Agnarsson, F. Magnus, T.K. Tryggvason, A.S. Ingason, K. Leosson, S. Olafsson, J. T. Gudmundsson, Rutile TiO 2 thin films grown by reactive high power impulse magnetron sputtering, Thin Solid Films. 545 (2013) 445–450, https://doi.org/10.1016/j.tsf.2013.07.058.
[17] T. Alasaarela, T. Saastamoinen, J. Hiltunen, A. Säynätjoki, A. Tervonen, P. Stenberg, M. Kuittinen, S. Honkanen, Atomic layer deposited titanium dioxide and its application in resonant waveguide grating, Appl. Opt. 49 (2010) 4321–4325, https://doi.org/10.1364/AO.49.004321.
[18] R.J.D. Tilley, Colour and the optical properties of materials: an exploration of the relationship between light, the optical properties of materials and colour, 2. Ed., Wiley, Chichester, 2011.
[19] A. Szeghalmi, M. Helgert, R. Brunner, F. Heyroth, U. Gösele, M. Knez, Atomic layer deposition of Al_2O_3 and TiO_2 multilayers for applications as bandpass filters and antireflection coatings, Appl. Opt. 48 (2009) 1727–1732, https://doi.org/10.1364/AO.48.001727.
[20] Y. Liu, Y. Yang, Recent Progress of TiO2-Based Anodes for Li Ion Batteries, J. Nanomater. 2016 (2016) e8123652. https://doi.org/10.1155/2016/8123652.
[21] H. Sopha, G.D. Salian, R. Zazpe, J. Prikryl, L. Hromadko, T. Djenizian, J.M. Macak, ALD Al $_{2}$ $_{O}$ 3 -Coated Ti$_{O}$ 2 Nanotube Layers as Anodes for Lithium-Ion Batteries, ACS Omega. 2 (2017) 2749–2756, https://doi.org/10.1021/acsomega.7b00463.
[22] J. Robertson, High dielectric constant oxides, Eur. Phys. J. - Appl. Phys. 28 (2004) 265–291, https://doi.org/10.1051/epjap:2004206.
[23] A. Kahouli, M.B. Elbahri, O. Lebedev, U. Lüders, Capacitance–voltage characteristics of sub-nanometric Al $_{2}$ $_{O}$ 3 / Ti$_{O}$ 2 laminates: dielectric and interface charge densities, J. Phys. Condens. Matter. 29 (2017), 275301, https://doi.org/10.1088/1361-648X/aa7237.
[24] G.D. Wilk, R.M. Wallace, J.M. Anthony, High-κ gate dielectrics: Current status and materials properties considerations, J. Appl. Phys. 89 (2001) 5243–5275, https://doi.org/10.1063/1.1361065.
[25] S.K. Kim, W.-D. Kim, K.-M. Kim, C.S. Hwang, J. Jeong, High dielectric constant TiO2 thin films on a Ru electrode grown at 250 °C by atomic-layer deposition, Appl. Phys. Lett. 85 (2004) 4112–4114, https://doi.org/10.1063/1.1812832.

[26] J.Y. Kim, D.-W. Kim, H.S. Jung, K.S. Hong, Influence of Anatase-Rutile Phase Transformation on Dielectric Properties of Sol-Gel Derived TiO $_2$ Thin Films, Jpn. J. Appl. Phys. 44 (2005) 6148–6151, https://doi.org/10.1143/JJAP.44.6148.

[27] R. van de Krol, A. Goossens, J. Schoonman, Mott-Schottky Analysis of Nanometer-Scale Thin-Film Anatase TiO2, J. Electrochem. Soc. 144 (5) (1997) 1723–1727.

[28] J.H. Shim, H.J. Choi, Y. Kim, J. Torgersen, J. An, M.H. Lee, F.B. Prinz, Process–property relationship in high-k ALD SrTiO 3 and BaTiO 3: a review, J. Mater. Chem. C. 5 (2017) 8000–8013, https://doi.org/10.1039/C6TC05158H.

[29] J.-H. Choi, S.-H. Kwon, Y.-K. Jeong, I. Kim, K.-H. Kim, Atomic Layer Deposition of Ta-doped TiO2 Electrodes for Dye-Sensitized Solar Cells, J. Electrochem. Soc. 158 (2011) B749, https://doi.org/10.1149/1.3582765.

[30] V. Pore, M. Heikkilä, M. Ritala, M. Leskelä, S. Areva, Atomic layer deposition of TiO2−xNx thin films for photocatalytic applications, J. Photochem. Photobiol. Chem. 177 (2006) 68–75, https://doi.org/10.1016/j.jphotochem.2005.05.013.

[31] J.-P. Niemelä, G. Marin, M. Karppinen, Titanium dioxide thin films by atomic layer deposition: a review, Semicond. Sci. Technol. 32 (9) (2017) 093005.

[32] D.S. Ginley, (Ed.), Handbook of Transparent Conductors, Springer US, Boston, MA, 2011. https://doi.org/10.1007/978-1-4419-1638-9.

[33] N. Inoue, H. Yuasa, M. Okoshi, TiO2 thin films prepared by PLD for photocatalytic applications, Appl. Surf. Sci. 197–198 (2002) 393–397, https://doi.org/10.1016/S0169-4332(02)00347-1.

[34] Y. Suda, H. Kawasaki, T. Ueda, T. Ohshima, Preparation of high quality nitrogen doped TiO2 thin film as a photocatalyst using a pulsed laser deposition method, Thin Solid Films. 453–454 (2004) 162–166, https://doi.org/10.1016/j.tsf.2003.11.185.

[35] S. Tanemura, L. Miao, W. Wunderlich, M. Tanemura, Y. Mori, S. Toh, K. Kaneko, Fabrication and characterization of anatase/rutile–TiO $_2$ thin films by magnetron sputtering: a review, Sci. Technol. Adv. Mater. 6 (2005) 11–17, https://doi.org/10.1016/j.stam.2004.06.003.

[36] A. Zaleska, Doped-TiO2: A Review, Recent Pat. Eng. (2008) 157–164.

[37] U.G. Akpan, B.H. Hameed, The advancements in sol–gel method of doped-TiO2 photocatalysts, Appl. Catal. Gen. 375 (2010) 1–11, https://doi.org/10.1016/j.apcata.2009.12.023.

[38] M. Shakeel Ahmad, A.K. Pandey, N. Abd Rahim, Advancements in the development of TiO2 photoanodes and its fabrication methods for dye sensitized solar cell (DSSC) applications, A review, Renew. Sustain. Energy Rev. 77 (2017) 89–108, https://doi.org/10.1016/j.rser.2017.03.129.

[39] B.-C. Kang, S.-B. Lee, J.-H. Boo, Growth of TiO2 thin films on Si(100) substrates using single molecular precursors by metal organic chemical vapor deposition, Surf. Coat. Technol. 131 (2000) 88–92, https://doi.org/10.1016/S0257-8972(00)00765-9.

[40] E. Shkondin, O. Takayama, J.M. Lindhard, P.V. Larsen, M.D. Mar, F. Jensen, A. V. Lavrinenko, Fabrication of high aspect ratio TiO2 and Al2O3 nanogratings by atomic layer deposition, J. Vac. Sci. Technol. Vac. Surf. Films. 34 (3) (2016) 031605.

[41] V. Miikkulainen, M. Leskelä, M. Ritala, R.L. Puurunen, Crystallinity of inorganic films grown by atomic layer deposition: Overview and general trends, J. Appl. Phys. 113 (2) (2013) 021301.

[42] S.D. Elliott, Atomic-scale simulation of ALD chemistry, Semicond. Sci. Technol. 27 (7) (2012) 074008.

[43] J. Aarik, A. Aidla, T. Uustare, V. Sammelselg, Morphology and structure of TiO2 thin films grown by atomic layer deposition, J. Cryst. Growth. 148 (1995) 268–275, https://doi.org/10.1016/0022-0248(94)00874-4.

[44] J. Aarik, A. Aidla, T. Uustare, M. Ritala, M. Leskelä, Titanium isopropoxide as a precursor for atomic layer deposition: characterization of titanium dioxide growth process, Appl. Surf. Sci. 161 (2000) 385–395, https://doi.org/10.1016/S0169-4332(00)00274-9.

[45] V.R. Rai, S. Agarwal, Surface Reaction Mechanisms during Ozone-Based Atomic Layer Deposition of Titanium Dioxide, J. Phys. Chem. C. 112 (2008) 9552–9554, https://doi.org/10.1021/jp8028616.

[46] Q. Xie, J. Musschoot, D. Deduytsche, R.L.V. Meirhaeghe, C. Detavernier, S.V. den Berghe, Y.-L. Jiang, G.-P. Ru, B.-Z. Li, X.-P. Qu, Growth Kinetics and Crystallization Behavior of TiO2 Films Prepared by Plasma Enhanced Atomic Layer Deposition, J. Electrochem. Soc. 155 (2008) H688–H692, https://doi.org/10.1149/1.2955724.

[47] R.A. Levy, (Ed.), Microelectronic Materials and Processes, Springer Netherlands, Dordrecht, 1989. https://doi.org/10.1007/978-94-009-0917-5.

[48] J.T. Clemens, Silicon microelectronics technology, Bell Labs Tech. J. 2 (1997) 76–102, https://doi.org/10.1002/bltj.2084.

[49] T. Yao, X. An, H. Han, J.Q. Chen, C. Li, Photoelectrocatalytic Materials for Solar Water Splitting, Adv. Energy Mater. 8 (2018) 1800210, https://doi.org/10.1002/aenm.201800210.

[50] T. Hitosugi, N. Yamada, S. Nakao, Y. Hirose, T. Hasegawa, Properties of TiO2-based transparent conducting oxides, Phys. Status Solidi A. 207 (2010) 1529–1537, https://doi.org/10.1002/pssa.200983774.

[51] Y. Furubayashi, T. Hitosugi, Y. Yamamoto, K. Inaba, G.o. Kinoda, Y. Hirose, T. Shimada, T. Hasegawa, A transparent metal: Nb-doped anatase TiO2, Appl. Phys. Lett. 86 (25) (2005) 252101.

[52] G. Triani, P.J. Evans, D.R.G. Mitchell, D.J. Attard, K.S. Finnie, M. James, T. Hanley, B. Latella, K.E. Prince, J. Bartlett, Atomic layer deposition of TiO 2 / Al 2 O 3 films for optical applications, in: M.L. Fulton, J.D.T. Kruschwitz (Eds.), San Diego, California, USA, 2005: p. 587009. https://doi.org/10.1117/12.638039.

[53] E. Celik, I. Keskin, I. Kayatekin, F. Ak Azem, E. Özkan, Al2O3–TiO2 thin films on glass substrate by sol–gel technique, Mater. Charact. 58 (2007) 349–357, https://doi.org/10.1016/j.matchar.2006.05.015.

[54] R. Chen, J.-L. Lin, W.-J. He, C.-L. Duan, Q.i. Peng, X.-L. Wang, B. Shan, Spatial atomic layer deposition of ZnO/TiO2 nanolaminates, J. Vac. Sci. Technol. A. 34 (5) (2016) 051502.

[55] J. Felizco, T. Juntunen, M. Uenuma, J. Etula, C. Tossi, Y. Ishikawa, I. Tittonen, Y. Uraoka, Enhanced Thermoelectric Transport and Stability in Atomic Layer Deposited-HfO $_2$ /ZnO and TiO $_2$ /ZnO-Sandwiched Multilayer Thin Films, ACS Appl. Mater. Interfaces. 12 (2020) 49210–49218, https://doi.org/10.1021/acsami.0c11439.

[56] M. Law, L.E. Greene, A. Radenovic, T. Kuykendall, J. Liphardt, P. Yang, ZnO−Al2O3 and ZnO−TiO2 Core−Shell Nanowire Dye-Sensitized Solar Cells, J. Phys. Chem. B. 110 (2006) 22652–22663, https://doi.org/10.1021/jp0648644.

[57] S.K. Kim, S. Hoffmann-Eifert, M. Reiners, R. Waser, Relation Between Enhancement in Growth and Thickness-Dependent Crystallization in ALD TiO2 Thin Films, J. Electrochem. Soc. 158 (2010) D6, https://doi.org/10.1149/1.3507258.

[58] M. Kaipio, T. Blanquart, Y. Tomczak, J. Niinistö, M. Gavagnin, V. Longo, H. D. Wanzenböck, V.R. Pallem, C. Dussarrat, E. Puukilainen, M. Ritala, M. Leskelä, Atomic Layer Deposition, Characterization, and Growth Mechanistic Studies of TiO2 Thin Films, Langmuir. 30 (2014) 7395–7404, https://doi.org/10.1021/la500893u.

[59] W.-J. Lee, M.-H. Hon, Space-Limited Crystal Growth Mechanism of TiO $_2$ Films by Atomic Layer Deposition, J. Phys. Chem. C. 114 (2010) 6917–6921, https://doi.org/10.1021/jp911210q.

[60] R.L. Puurunen, T. Sajavaara, E. Santala, V. Miikkulainen, T. Saukkonen, M. Laitinen, M. Leskelä, Controlling the Crystallinity and Roughness of Atomic Layer Deposited Titanium Dioxide Films, J. Nanosci. Nanotechnol. 11 (2011) 8101–8107, https://doi.org/10.1166/jnn.2011.5060.

[61] V.-S. Dang, H. Parala, J.H. Kim, K.e. Xu, N.B. Srinivasan, E. Edengeiser, M. Havenith, A.D. Wieck, T. de los Arcos, R.A. Fischer, A. Devi, Electrical and optical properties of TiO2 thin films prepared by plasma-enhanced atomic layer deposition, Phys. Status Solidi A. 211 (2) (2014) 416–424.

[62] M.-H. Jang, Y.u. Lei, Ultrasonic atomization of titanium isopropoxide at room temperature for TiO $_2$ atomic layer deposition, J. Vac. Sci. Technol. A. 38 (6) (2020) 062405.

[63] W. Chiappim, M.A. Fraga, H.S. Maciel, R.S. Pessoa, An Experimental and Theoretical Study of the Impact of the Precursor Pulse Time on the Growth Per Cycle and Crystallinity Quality of TiO2 Thin Films Grown by ALD and PEALD Technique, Front. Mech. Eng. 6 (2020), 551085, https://doi.org/10.3389/fmech.2020.551085.

[64] R.L. Puurunen, W. Vandervorst, Island growth as a growth mode in atomic layer deposition: A phenomenological model, J. Appl. Phys. 96 (2004) 7686–7695, https://doi.org/10.1063/1.1810193.

[65] R.L. Puurunen, Surface chemistry of atomic layer deposition: A case study for the trimethylaluminum/water process, J. Appl. Phys. 97 (12) (2005) 121301.

[66] R.S. Pessoa, F.P. Pereira, G.E. Testoni, W. Chiappim, H.S. Maciel, L.V. Santos, Effect of substrate type on structure of TiO2 thin film deposited by atomic layer deposition technique, J. Integr. Circuits Syst. 10 (2015) 38–42, https://doi.org/10.29292/jics.v10i1.403.

[67] R.J. Gonzalez, R. Zallen, H. Berger, Infrared reflectivity and lattice fundamentals in anatase ${\mathrm{TiO}}_{2}$s, Phys. Rev. B. 55 (1997) 7014–7017, https://doi.org/10.1103/PhysRevB.55.7014.

[68] A. Miquelot, O. Debieu, V. Rouessac, C. Villeneuve, N. Prud'homme, J. Cure, V. Constantoudis, G. Papavieros, S. Roualdes, C. Vahlas, TiO2 nanotree films for the production of green H2 by solar water splitting: From microstructural and optical characteristics to the photocatalytic properties, Appl. Surf. Sci. 494 (2019) 1127–1137.

[69] N. Primeau, C. Vautey, M. Langlet, The effect of thermal annealing on aerosol-gel deposited SiO2 films: a FTIR deconvolution study, Thin Solid Films. 310 (1997) 47–56, https://doi.org/10.1016/S0040-6090(97)00340-4.

[70] A.J. Henegar, T. Gougousi, Stability and Surface Reactivity of Anatase TiO 2 Films, ECS J. Solid State Sci. Technol. 4 (8) (2015) P298–P304.

[71] L. Ferretto, A. Glisenti, Surface Acidity and Basicity of a Rutile Powder, Chem. Mater. 15 (2003) 1181–1188, https://doi.org/10.1021/cm021269f.

[72] C. Morterra, An infrared spectroscopic study of anatase properties. Part 6.—Surface hydration and strong Lewis acidity of pure and sulphate-doped preparations, J. Chem. Soc., Faraday Trans. 1 84 (5) (1988) 1617.

[73] M.E. Dufond, M.W. Diouf, C. Badie, C. Laffon, P. Parent, D. Ferry, D. Grosso, J.C. S. Kools, S.D. Elliott, L. Santinacci, Quantifying the Extent of Ligand Incorporation and the Effect on Properties of TiO2 Thin Films Grown by Atomic Layer Deposition Using an Alkoxide or an Alkylamide, Chem Mater. 32 (4) (2020) 1393–1407.

[74] D. Saha, R.S. Ajimsha, K. Rajiv, C. Mukherjee, M. Gupta, P. Misra, L.M. Kukreja, Spectroscopic ellipsometry characterization of amorphous and crystalline TiO 2 thin films grown by atomic layer deposition at different temperatures, Appl. Surf. Sci. 315 (2014) 116–123, https://doi.org/10.1016/j.apsusc.2014.07.098.

[75] D.R.G. Mitchell, G. Triani, D.J. Attard, K.S. Finnie, P.J. Evans, C.J. Barbé, J. R. Bartlett, Atomic layer deposition of TiO $_2$ and Al $_2$ O 3 thin films and nanolaminates, Smart Mater. Struct. 15 (2006) S57–S64, https://doi.org/10.1088/0964-1726/15/1/010.

[76] D.R.G. Mitchell, D.J. Attard, G. Triani, Transmission electron microscopy studies of atomic layer deposition TiO2 films grown on silicon, Thin Solid Films. 441 (2003) 85–95, https://doi.org/10.1016/S0040-6090(03)00877-0.

[77] T. Ohsaka, F. Izumi, Y. Fujiki, Raman spectrum of anatase, TiO2, J. Raman Spectrosc. 7 (1978) 321–324, https://doi.org/10.1002/jrs.1250070606.

[78] D. Tuschel, The Correlation Method for the Determination of Spectroscopically Active Vibrational Modes in Crystals, (n.d.).

[79] X. Nie, F. Ma, D. Ma, K. Xu, Thermodynamics and kinetic behaviors of thickness-dependent crystallization in high-k thin films deposited by atomic layer deposition, J. Vac. Sci. Technol. Vac. Surf. Films. 33 (2015) 01A140, https://doi.org/10.1116/1.4903946.

[80] J. Aarik, A. Aidla, A.-A. Kiisler, T. Uustare, V. Sammelselg, Effect of crystal structure on optical properties of TiO2 films grown by atomic layer deposition, Thin Solid Films. 305 (1997) 270–273, https://doi.org/10.1016/S0040-6090(97)00135-1.

[81] L. Aarik, T. Arroval, R. Rammula, H. Mändar, V. Sammelselg, J. Aarik, Atomic layer deposition of TiO2 from TiCl4 and O3, Thin Solid Films. 542 (2013) 100–107, https://doi.org/10.1016/j.tsf.2013.06.074.

[82] M.H. Suhail, G.M. Rao, S. Mohan, dc reactive magnetron sputtering of titanium-structural and optical characterization of TiO $_2$ films, J. Appl. Phys. 71 (1992) 1421–1427, https://doi.org/10.1063/1.351264.

[83] Y.-J. Shi, R.-J. Zhang, H. Zheng, D.-H. Li, W. Wei, X. Chen, Y. Sun, Y.-F. Wei, H.-L. Lu, N. Dai, L.-Y. Chen, Optical Constants and Band Gap Evolution with Phase Transition in Sub-20-nm-Thick TiO2 Films Prepared by ALD, Nanoscale Res. Lett. 12 (2017) 243, https://doi.org/10.1186/s11671-017-2011-2.

[84] M. Horprathum, P. Eiamchai, P. Limnonthakul, N. Nuntawong, P. Chindaudom, A. Pokaipisit, P. Limsuwan, Structural, optical and hydrophilic properties of nanocrystalline TiO2 ultra-thin films prepared by pulsed dc reactive magnetron sputtering, J. Alloys Compd. 509 (2011) 4520–4524, https://doi.org/10.1016/j.jallcom.2011.01.038.

[85] B.D. Piercy, C.Z. Leng, M.D. Losego, Variation in the density, optical polarizabilities, and crystallinity of TiO2 thin films deposited via atomic layer deposition from 38 to 150 °C using the titanium tetrachloride-water reaction, J. Vac. Sci. Technol. A. 35 (2017) 03E107, https://doi.org/10.1116/1.4979047.

[86] T. Busani, R.A.B. Devine, Dielectric and infrared properties of TiO $_2$ films containing anatase and rutile, Semicond. Sci. Technol. 20 (2005) 870–875, https://doi.org/10.1088/0268-1242/20/8/043.

[87] M.B. Elbahri, A. Kahouli, B. Mercey, W. Prellier, U. Lüders, Effects of oxygen pressure during deposition on the dielectric properties of amorphous titanium dioxide thin films, J. Phys. Appl. Phys. 52 (17) (2019) 175308.

[88] W. Chen, W. Ren, Y. Zhang, M. Liu, Z.-G. Ye, Preparation and properties of ZrO2 and TiO2 films and their nanolaminates by atomic layer deposition, Ceram. Int. 41 (2015) S278–S282, https://doi.org/10.1016/j.ceramint.2015.03.257.

[89] D. Mardare, G.I. Rusu, Comparison of the dielectric properties for doped and undoped TiO2 thin films, J. Optoelectron. Adv. Mater. 6 (2003) 333–336.

[90] M.D. Stamate, On the dielectric properties of dc magnetron TiO2 thin films, Appl. Surf. Sci. 218 (2003) 318–323, https://doi.org/10.1016/S0169-4332(03)00624-X.